FULL PAPER

Dalton
www.rsc.org/dalton

Tuning facial–meridional isomerisation in monometallic nine-co-ordinate lanthanide complexes with unsymmetrical tridentate ligands †

Thierry Le Borgne,[a] Peter Altmann,[a] Nicolas André,[b] Jean-Claude G. Bünzli,*[b] Gérald Bernardinelli,[c] Pierre-Yves Morgantini,[d] Jacques Weber[d] and Claude Piguet*[a]

[a] *Department of Inorganic, Analytical and Applied Chemistry, University of Geneva, 30 quai E. Ansermet, CH-1211 Geneva 4, Switzerland. E-mail: Claude.Piguet@chiam.unige.ch*

[b] *Institute of Molecular and Biological Chemistry, Swiss Federal Institute of Technology, BCH 1402, CH-1015 Lausanne, Switzerland. E-mail: Jean-Claude.Bunzli@epfl.ch*

[c] *Laboratory of X-ray Crystallography, 24 quai E. Ansermet, CH-1211 Geneva 4, Switzerland*

[d] *Department of Physical Chemistry, University of Geneva, 30 quai E. Ansermet, CH-1211 Geneva 4, Switzerland*

Received 9th December 2003, Accepted 7th January 2004
First published as an Advance Article on the web 30th January 2004

The unsymmetrical tridentate benzimidazole–pyridine–carboxamide units in ligands **L1**–**L4** react with trivalent lanthanides, Ln^{III}, to give the nine-co-ordinate triple-helical complexes $[Ln(\mathbf{Li})_3]^{3+}$ (i=1–4) existing as mixtures of C_3-symmetrical facial and C_1-symmetrical meridional isomers. Although the β_{13} formation constants are 3–4 orders of magnitude smaller for these complexes than those found for the D_3-symmetrical analogues $[Ln(\mathbf{Li})_3]^{3+}$ (i=5–6) with symmetrical ligands, their formation at the millimolar scale is quantitative and the emission quantum yield of $[Eu(\mathbf{L2})_3]^{3+}$ is significantly larger. The *fac*-$[Ln(\mathbf{Li})_3]^{3+} \rightleftharpoons$ *mer*-$[Ln(\mathbf{Li})_3]^{3+}$ (i=1–4) isomerisation process in acetonitrile is slow enough for Ln=Lu^{III} to be quantified by ^{1}H NMR below room temperature. The separation of enthalpic and entropic contributions shows that the distribution of the facial and meridional isomers can be tuned by the judicious peripheral substitution of the ligands affecting the interstrand interactions. Molecular mechanics (MM) calculations suggest that one supplementary interstrand π-stacking interaction stabilises the meridional isomers, while the facial isomers benefit from more favourable electrostatic contributions. As a result of the mixture of facial and meridional isomers in solution, we were unable to obtain single crystals of 1 : 3 complexes, but the X-ray crystal structures of their nine-co-ordinate precursors $[Eu(\mathbf{L1})_2(CF_3SO_3)_2(H_2O)](CF_3SO_3)(C_3H_5N)_2(H_2O)$ (**6**, $C_{45}H_{54}EuF_9N_{10}O_{13}S_3$, monoclinic, $P2_1/c$, Z=4) and $[Eu(\mathbf{L4})_2(CF_3SO_3)_2(H_2O)](CF_3SO_3)(C_4H_4O)_{1.5}$ (**7**, $C_{51}H_{66}EuF_9N_8O_{15.5}S_3$, triclinic, $P\bar{1}$, Z=2) provide crucial structural information on the binding mode of the unsymmetrical tridentate ligands.

Introduction

Since the early time of co-ordination chemistry,[1] the selective preparation of different isomers of pseudo-octahedral tris-chelates of transition metals $[M\mathbf{L}_3]^{n+}$ is a theme of continuous significance,[2] as are the mechanisms of their interconversion.[3] For C_2-symmetrical bidentate chelates possessing two equivalent donor sites, a single pair of D_3-symmetrical helical enantiomers results (*P*-$[M\mathbf{L}_3]^{n+}$ and *M*-$[M\mathbf{L}_3]^{n+}$), and their diastereomeric separation after interaction with a chiral partner (often with an enantiomerically pure counterion) can be achieved when $[M\mathbf{L}_3]^{n+}$ is kinetically inert (M = Ru^{II}, Co^{III}, Ir^{III}).[4] For unsymmetrical bidentate ligands possessing two different donor sites, the tris-chelates may exist as two pairs of enantiomers: *fac*-*P*-$[M\mathbf{L}_3]^{n+}$/*fac*-*M*-$[M\mathbf{L}_3]^{n+}$ and *mer*-*P*-$[M\mathbf{L}_3]^{n+}$/*mer*-*M*-$[M\mathbf{L}_3]^{n+}$ in which *fac* stands for the C_3-symmetrical facial isomer (three ligands with parallel orientations) and *mer* for the C_1-symmetrical meridional isomer (one ligand adopts the opposite orientation).[5] Therefore, it is often difficult to isolate pure isomers with unsymmetrical bidentate ligands, and this strongly limits the preparation of metallosupramolecular architectures with predetermined stereochemistry and functions.[2,3,6] Surprisingly, the analogous isomerisation process occurring in lanthanide-containing tris-chelates with tridentate ligands and pseudo-tricapped trigonal prismatic geometry $[Ln\mathbf{L}_3]^{3+}$ has been only marginally investigated, except for the *P*/*M* helical interconversion in $[Ln(2,6\text{-dipicolinate})_3]^{3-}$ for which rate constants k_{rac}^{298} = 50–200 s^{-1} have been reported.[7] This suggests that the different isomers of nine-co-ordinate $[Ln\mathbf{L}_3]^{3+}$ complexes are too labile to be separated on the laboratory scale, but that *P*/*M* and/or *fac*/*mer* isomerisation with tridentate ligands can be investigated with ^{1}H-NMR techniques.[7] In this context, variable-temperature NMR studies of the *fac*-$[Ln\mathbf{L}_3]^{3+} \rightleftharpoons$ *mer*-$[Ln\mathbf{L}_3]^{3+}$ interconversion (Fig. 1) should provide thermodynamic and kinetic parameters which are crucial for (i) programming lanthanide co-ordination spheres with predetermined crystal-fields,[8] (ii) tuning the intramolecular interstrand interactions responsible for selective complexation along the lanthanide series[9] and (iii) modelling deviations from a binomial distribution for the formation of *HHH versus HHT* bimetallic triple-stranded lanthanide helicates.[10]

In this contribution, we report on the structural and thermodynamic investigation of the *fac*-$[Ln(\mathbf{Li})_3]^{3+} \rightleftharpoons$ *mer*-$[Ln(\mathbf{Li})_3]^{3+}$ interconversion process (i = 1–4) in which peripheral substitution of the tridentate benzimidazole–pyridine–carboxamide unit is expected to modulate interstrand interactions. We have proposed that the unprecedented selectivity observed for mid-range lanthanides in $[Ln(\mathbf{L5})_3]^{3+}$ results from specific intramolecular interstrand aromatic π-stacking interactions.[9a] Therefore the stepwise connection of bulky substituents in going from **L1** to **L3** is expected to reduce interstrand stacking

† Electronic supplementary information (ESI) available: Luminescence data for $[Eu(\mathbf{L2})_3]^{3+}$ and $[Tb(\mathbf{L2})_3]^{3+}$ (Table S1), elemental analyses (Table S2), structural data for the lanthanide co-ordination sphere in $[Eu(\mathbf{L1})_2(CF_3SO_3)_2(H_2O)](CF_3SO_3)(C_3H_5N)_2(H_2O)$ (**6**) and $[Eu(\mathbf{L4})_2(CF_3SO_3)_2(H_2O)](CF_3SO_3)(THF)_{1.5}$ (**7**) (Table S3); an optimised superimposition of the two molecular structures of $[Eu(\mathbf{L5})_3]^{3+}$ (X-ray and calculated in the gas phase, Fig. S1), perspective views of the molecular structures of *fac*-$[Lu(\mathbf{L3})_3]^{3+}$ and *mer*-$[Lu(\mathbf{L3})_3]^{3+}$ (Fig. S2) and *fac*-$[Lu(\mathbf{L4})_3]^{3+}$ and *mer*-$[Lu(\mathbf{L4})_3]^{3+}$ (Fig. S3) obtained by molecular mechanics in the gas-phase. See http://www.rsc.org/suppdata/dt/b3/b316035a/

DOI: 10.1039/b316035a

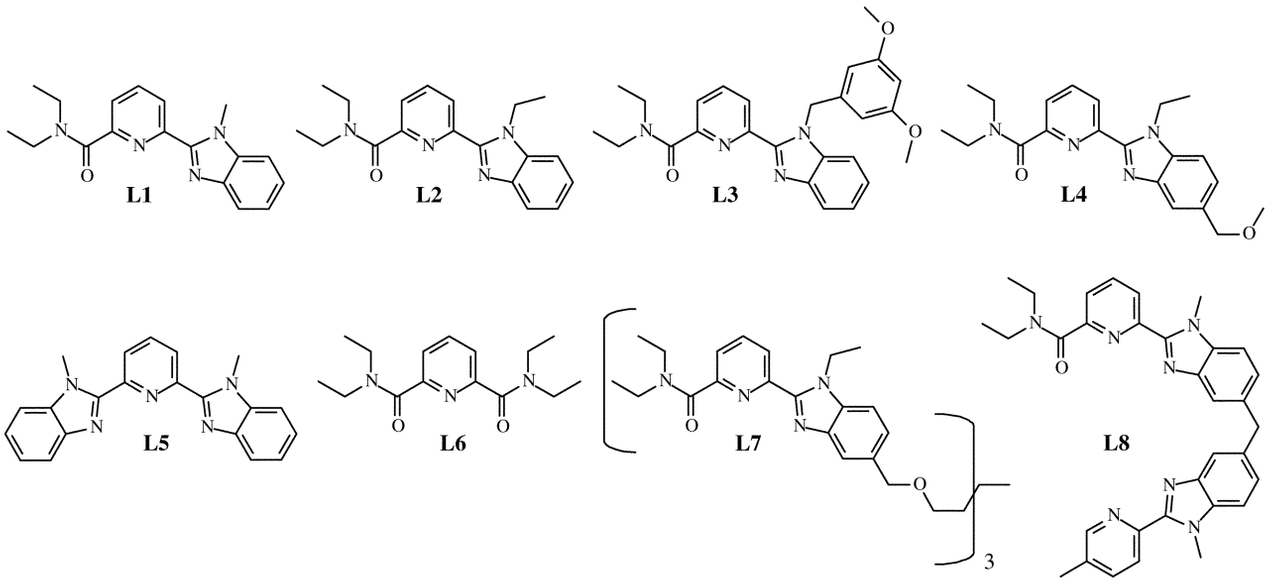

Scheme 1 Structures of the ligands **L1**–**L8**.

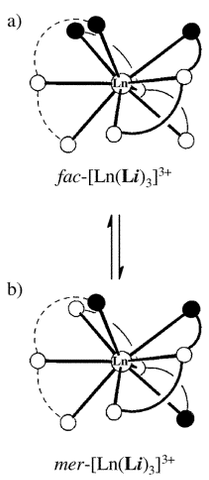

Fig. 1 Schematic representation of (a) the C_3-symmetrical facial, *fac*-$[Ln(\mathbf{L}i)_3]^{3+}$, and (b) the C_1-symmetrical meridional, *mer*-$[Ln(\mathbf{L}i)_3]^{3+}$, stereo-isomers in nine-co-ordinate monometallic lanthanide complexes with three unsymmetrical tridentate ligands (**L1**–**L4**; the black circles correspond to the oxygen donor atoms of the carboxamide side arms).

in *mer*-$[Ln(\mathbf{L}i)_3]^{3+}$, leading to its destabilisation with respect to *fac*-$[Ln(\mathbf{L}i)_3]^{3+}$ for which no interstrand stacking is possible. Finally, the comparison between $[Ln(\mathbf{L1})_3]^{3+}$ and $[Ln(\mathbf{L4})_3]^{3+}$ will explore the effect of substitution at the 5-position of the benzimidazole ring, a structural pattern commonly used for preparing bimetallic lanthanide helicates.[10]

Results and discussion

Complexation properties of L1–L4 with trivalent lanthanide cations (Ln = La–Lu)

The tridentate ligands **L1**–**L4** correspond to key intermediates during the syntheses of extended segmental ligands, and they are obtained in fair to good yields.[11–13] As reported for the podand **L7**, which possesses three tridentate **L4** binding units facially connected to a covalent tripod (Scheme 1),[13] the electronic absorption spectra are dominated by ligand-centred n,π⟶π* transitions in the 230–400 nm range which are globally red-shifted by ≈ 1800 cm^{-1} upon complexation to Ln^{III} (Fig. 2a), thus allowing a quantitative analysis of the thermodynamic complexation process by using spectrophotometric titrations (Fig. 2b).

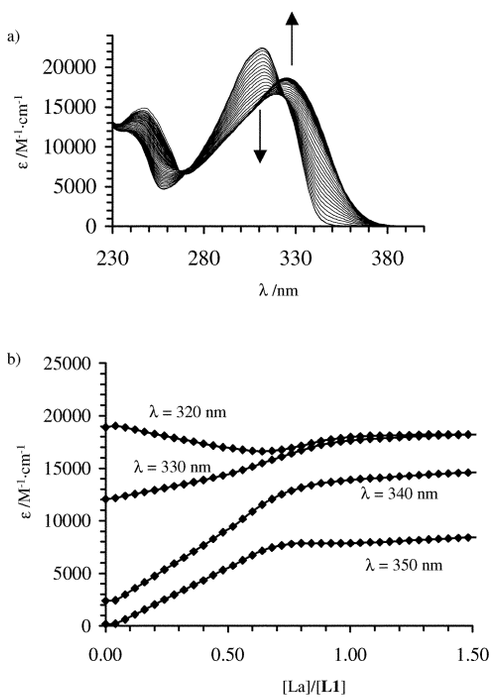

Fig. 2 (a) Variation of absorption spectra observed for the spectrophotometric titration of **L1** (2 10^{-4} mol dm^{-3} in acetonitrile) with $La(ClO_4)_3 \cdot 6H_2O$ at 293 K (La : **L1** = 0.1–1.5). (b) Corresponding variation of observed molar extinctions at four different wavelengths.

Titrations of **L1**–**L4** (2 10^{-4} mol dm^{-3}) with $Ln(ClO_4)_3 \cdot xH_2O$ (Ln = La, Pr, Eu, Gd, Dy, Er, Lu, x = 1–8; Ln : **L***i* = 0.1–1.5) in acetonitrile show a smooth and intricate evolution of the absorption spectra with one final end point for Ln : **L***i* = 1.0. Factor analysis[14] systematically confirms the formation of four absorbing species assigned to **L***i* and $[Ln(\mathbf{L}i)_n]^{3+}$ (n = 1–3) as previously established for **L5**[9,15] and **L6**.[16] The spectrophotometric data can be satisfyingly fitted with non-linear least-squares techniques[17] to equilibria (1)–(3), and the associated formation constants are collected in Table 1.

$$Ln^{3+} + \mathbf{L}i \rightleftharpoons [Ln(\mathbf{L}i)]^{3+} \quad \log(\beta_{11}^{Ln}) \qquad (1)$$

$$Ln^{3+} + 2\,\mathbf{L}i \rightleftharpoons [Ln(\mathbf{L}i)_2]^{3+} \quad \log(\beta_{12}^{Ln}) \qquad (2)$$

$$Ln^{3+} + 3\,\mathbf{L}i \rightleftharpoons [Ln(\mathbf{L}i)_3]^{3+} \quad \log(\beta_{13}^{Ln}) \qquad (3)$$

Table 1 Cumulative stability constants log (β_{ln}^{Ln}) for $[Ln(\mathbf{Li})_n]^{3+}$ (i=1–6, n=1–3, acetonitrile, 293 K)

		L1			L2[a]			L3			L4			L5[c]			L6[d]	
Metal	R^{Ln}/Å[b]	log(β_{11})	log(β_{12})	log(β_{13})	log(β_{11})	log(β_{12})	log(β_{13})	log(β_{11})	log(β_{12})	log(β_{13})	log(β_{11})	log(β_{12})	log(β_{13})	log(β_{11})	log(β_{12})	log(β_{13})	log(β_{11})	log(β_{12})	log(β_{13})
La(III)	1.216	7.1(3)	11.6(4)	15.9(5)	8.6(3)	15.1(4)	19.9(4)	6.7(2)	11.7(3)	17.1(4)	7.3(3)	12.7(4)	17.0(5)	8.9(3)	16.8(4)	23.3(9)	7.4(3)	14.8(3)	21.0(3)
Pr(III)	1.179	7.7(3)	13.7(5)	17.8(6)				7.6(4)	13.2(5)	17.6(7)				8.7(2)[e]	15.9(4)[e]	23.2(8)[e]	7.6(3)	14.6(3)	22.2(3)
Eu(III)	1.120				7.8(2)	13.5(2)	19.2(2)							9.0(2)	15.7(3)	22.6(6)	8.3(3)	15.3(3)	22.3(3)
Gd(III)	1.107	7.3(2)	12.3(3)	17.4(4)				7.0(2)	11.8(3)	17.0(5)	7.6(4)	12.8(5)	18.0(7)	8.5(2)	15.2(4)	22.1(8)	7.9(3)	14.7(4)	22.6(4)
Dy(III)	1.083	7.4(3)	12.5(4)	16.5(5)				7.7(3)	12.4(4)	16.9(5)				8.9(3)[f]	16.2(5)[f]	22(1)[f]	7.5(3)	14.8(4)	22.5(4)
Er(III)	1.062	8.0(4)	13.2(4)	17.9(5)				7.8(3)	12.7(3)	17.1(3)				9.4(5)[g]	16.5(6)[g]	21(1)[g]	7.7(4)	14.4(4)	22.7(4)
Lu(III)	1.032	7.2(2)	11.5(4)	17.3(4)	9.2(2)	16.8(4)	21.9(4)	7.2(2)	12.7(3)	18.5(5)	7.0(8)	11.9(8)	17.5(7)	9.0(4)	15.4(4)	20.3(9)	8.1(3)	15.2(3)	22.9(3)

[a] Anhydrous $Ln(ClO_4)_3$ have been used for titrations with **L2** (see text). [b] Ionic radii for nine-co-ordinate Ln^{III}.[45] [c] Taken from ref. 9a. [d] Taken from ref. 16. [e] Measured for Ln = Nd. [f] Measured for Ln = Ho. [g] Measured for Ln = Yb.

Titrations of **L1**, **L3**–**L6** have been performed under the same experimental conditions by using hydrated lanthanide perchlorate salts $Ln(ClO_4)_3 \cdot xH_2O$ (x = 6–8) which provide approximately 50 ppm of additional water in distilled acetonitrile at the end of the titration. Therefore, comparison between these ligands is adequate, and Table 1 indicates that the formation constants β_{ln}^{Ln} (n = 1–3) with the unsymmetrical ligands **L1**, **L3** and **L4** are systematically smaller by 3–4 orders of magnitude than those reported for the symmetrical analogues **L5**[9a] and **L6**.[16] However, no significant size-discriminating effect can be detected along the lanthanide series except for the expected weak electrostatic trend (Fig. 3).[18]

Fig. 3 Cumulative stability constants log(β_{13}^{Ln}) for the formation of $[Ln(\mathbf{Li})_3]^{3+}$ (i=1: ◆, i=3: ■, i=4: ▲, i=5: ×, i=6: ●) *versus* the inverse of nine-co-ordinate lanthanide radii (R^{-1})[45] (acetonitrile, 293 K). The dotted trend-lines are only guides for the eyes.

Obviously, $[Ln(\mathbf{Li})_3]^{3+}$ (i = 1–4) species exist in solution as mixtures of facial and meridional isomers displaying slightly different absorption spectra, but this has been neglected for the calculation of the formation constants given in Table 1. However, we do not expect drastic differences between the free energies of formation of *fac*-$[Ln(\mathbf{Li})_3]^{3+}$ and *mer*-$[Ln(\mathbf{Li})_3]^{3+}$and, according to a statistical approach, we expect $\Delta(\Delta G^0_{formation}) = \Delta G^0_f(mer) - \Delta G^0_f(fac) = \Delta G^0_4 = -2.7$ kJ mol^{-1} (see eqn. 4, below), which is negligible compared with the average $\Delta G^0_{formation} = -RT\ln(\beta^{Ln}_{13}) = -97$ kJ mol^{-1} observed for these complexes. This indeed cannot account for the considerable decrease of $\Delta(\Delta G^0_{formation}) = \Delta G^0_f$ (*sym*) − ΔG^0_f (*unsym*) ≈ −28 kJ mol^{-1} observed in going from symmetrical (**L5**, **L6**) to unsymmetrical tridentate ligands (**L1**, **L3**, **L4**). For **L2**, a close analogue of **L1**, strictly anhydrous conditions have been used ($Ln(ClO_4)_3 \cdot xH_2O$, $x \leq 1$), and we indeed observe slightly larger formation constants which, however, remain smaller than those reported for **L5** and **L6**. Whatever the origin of the low stability of $[Ln(\mathbf{Li})_3]^{3+}$ (i = 1–4) is, we calculate that these complexes are quantitatively formed (>98%) under stoichiometric conditions at millimolar concentrations in acetonitrile.

Photophysical properties of $[Ln(L2)_3]^{3+}$ in acetonitrile (Ln = Eu, Tb, Lu)

The free ligand **L2** in acetonitrile (10^{-5} mol dm^{-3}, 295 K) displays a broad and asymmetric absorption band envelope centred at 31950 cm^{-1}, assigned to n,π⟶π* transitions (ε = 22000 M^{-1} cm^{-1}, Fig. 2a), and which closely matches that reported for **L7** (31650 cm^{-1}, ε/3 = 20000 M^{-1} cm^{-1}).[13] Excitation in this band (ν_{exc} = 31950 cm^{-1}) produces a broad and intense emission band at 27030 cm^{-1} (295 K) which can be ascribed to $^1\pi\pi^*$ fluorescence since the use of a 80 μs delay leads to the disappearance of this signal. At 77 K, in frozen acetonitrile, the time-delayed spectrum exemplifies a very weak and long-lived emission originating from the $^3\pi\pi^*$ state (0-phonon transition at 20830 cm^{-1}, $\tau \geq 100$ ms, Table S1, ESI †). Interestingly, the fluorescence quantum yield of **L2** (ϕ_f = 0.35(7), acetonitrile, 295 K) is significantly smaller than $\phi_f \approx 1.0$ reported for the symmetrical ligand **L5** in similar conditions,[19]

which suggests that the replacement of one rigid terminal benzimidazole side arm in **L5** with a *N*,*N*′-diethylcarboxamido group in **L2** favours vibrational quenching of the $^1\pi\pi^*$ level and/or improves intersystem crossing (ISC). Upon complexation to diamagnetic Lu^{III} in $[Lu(\mathbf{L2})_3]^{3+}$ (6 10^{-4} mol dm^{-3}, 295 K), the ligand-centred absorption (Fig. 2a) and $^1\pi\pi^*$ emission (24510 cm^{-1}, Fig. 4a) are red-shifted by 1800 and 2520 cm^{-1}, respectively. The time-delayed (10 μs) phosphorescence spectrum (frozen acetonitrile, 77 K) reveals the weak and structured asymmetric band characteristic of the emission of $^3\pi\pi^*$ (0–0 phonon at 20660 cm^{-1}, τ = 130(15) ms, Fig. 4b and Table S1, ESI). The ratio of the intensities $^3\pi\pi^*/^1\pi\pi^*$ significantly increases when going from **L2** to $[Lu(\mathbf{L2})_3]^{3+}$ as a result of the mixing of the singlet and triplet wavefunctions by the large spin–orbit coupling constant of Lu^{III}.[20] This behaviour strictly parallels that found for $[Gd(\mathbf{L7})]^{3+}$ ($E(^1\pi\pi^*)$ = 24180 cm^{-1}, $E(^3\pi\pi^*)$ = 20410 cm^{-1}) which possesses the same LnN_6O_3 metallic centre adopting exclusively a facial arrangement.[13] Irradiation of the ligand-centred $\pi\longrightarrow\pi^*$ transition of $[Eu(\mathbf{L2})_3]^{3+}$ (ν_{exc} = 37040 cm^{-1}, frozen acetonitrile, 77 K) shows the concomitant emission of the short-lived ligand-centred $^1\pi\pi^*$ excited state together with the long-lived Eu-centred $^5D_0\longrightarrow{}^7F_J$ (J = 1–4) transitions (Fig. 4c, Table S1, ESI).[21] The disappearance of the emission of the triplet state in $[Eu(\mathbf{L2})_3]^{3+}$ points to an efficient $^3\pi\pi^*\longrightarrow Eu^{III}$ energy transfer process, but an inefficient $^1\pi\pi^*\longrightarrow{}^3\pi\pi^*$ ISC, since the absolute quantum yield originating from $^1\pi\pi^*$ still amounts to ϕ_f = 0.35(7) (acetonitrile, 295 K) as found for **L2,** within experimental error. The $Eu(^5D_0)$ lifetimes are long (1.86–2.25 ms, Table S1, ESI) and match $\tau(Eu(^5D_0))$ = 2.87(1) ms (acetonitrile, 293 K) found for $[Eu(\mathbf{L7})]^{3+}$.[13] This confirms that Eu^{III} in $[Eu(\mathbf{L2})_3]^{3+}$ is nine-co-ordinate by the three tridentate binding units, and that no solvent molecule interacts in the first co-ordination sphere. However, the mixture of *fac*-$[Eu(\mathbf{L2})_3]^{3+}$ and *mer*-$[Eu(\mathbf{L2})_3]^{3+}$ may explain the slightly larger Eu-centred quantum yield obtained upon ligand excitation ϕ_f = (5±1) 10^{-2} (ν_{exc} = 37040 cm^{-1}, acetonitrile, 295 K), which can be compared with ϕ_f = (6±1) 10^{-3} for $[Eu(\mathbf{L7})]^{3+}$.[13] **L2** is also able to sensitize Tb^{III} in $[Tb(\mathbf{L2})_3]^{3+}$ at low temperature ($\tau(Tb(^5D_4))$ = 1.22(4) ms, acetonitrile, 77 K, Fig. 4d, Table S1, ESI), but the small energy gap $\Delta E = E(^3\pi\pi^*) - E(^5D_4)$ = 20660 − 20490 = 170 cm^{-1} strongly favours thermally-activated $Tb\longrightarrow\mathbf{L2}(^3\pi\pi^*)$ back transfer which quenches Tb-centred luminescence at 295 K ($\tau(Tb(^5D_4))$ = 0029(1) ms, Table S1, ESI) as similarly described for $[Tb(\mathbf{L7})]^{3+}$.[13] It is worth noting that emission originating from $^1\pi\pi^*$ is also observed for $[Tb(\mathbf{L2})_3]^{3+}$, which confirms inefficient ISC processes.

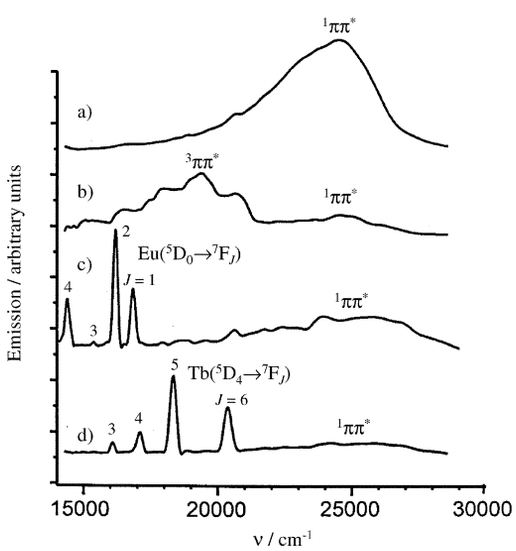

Fig. 4 Emission spectra of (a) $[Lu(\mathbf{L2})_3]^{3+}$ (delay time: 0 ms, 6 10^{-4} mol dm^{-3} in acetonitrile, ν_{exc} = 29600 cm^{-1}, 77 K); (b) $[Lu(\mathbf{L2})_3]^{3+}$ (delay time: 0.01 ms, 6 10^{-4} mol dm^{-3} in acetonitrile, ν_{exc} = 29600 cm^{-1}, 77 K); (c) $[Eu(\mathbf{L2})_3]^{3+}$ (delay time: 0 ms, 8 10^{-4} mol dm^{-3} in acetonitrile, ν_{exc} = 29600 cm^{-1}, 77 K); and (d) $[Tb(\mathbf{L2})_3]^{3+}$ (delay time: 0 ms, 8 10^{-4} mol dm^{-3} in acetonitrile, ν_{exc} = 29600 cm^{-1}, 77 K).

Isolation of $[Ln(L2)_3](ClO_4)_3\cdot xH_2O$ and $[Ln(L4)_3](CF_3SO_3)_3\cdot xC_7H_{15}$

Stoichiometric mixing of **L2** (3 eq) with $Ln(ClO_4)_3\cdot xH_2O$ (Ln = Eu, Tb, Lu, x = 1–3, 1 eq), or of **L4** (3 eqs) with $Ln(CF_3SO_3)_3\cdot xH_2O$ (Ln = Eu, Lu, x = 1–4, 1 eq) in acetonitrile provides amorphous powders with composition $[Ln(\mathbf{L2})_3](ClO_4)_3\cdot xH_2O$ (Ln = Eu, x = 4: **1**; Ln = Tb, x = 5.5: **2**; Ln = Lu, x = 4: **3**) and $[Ln(\mathbf{L4})_3](CF_3SO_3)_3\cdot xC_7H_{15}$ (Ln = Eu, x = 0: **4**; Ln = Lu, x = 0.4: **5**) after precipitation with diethyl ether (**1**–**3**) or heptane (**4**–**5**). Elemental analyses support the proposed formulations (Table S2, ESI †), and the IR spectra show the characteristic 30–35 cm^{-1} red-shift of the ν_{CO} vibration occurring upon complexation of the carboxamide groups to Ln^{III}, as previously reported for **L6**[16] and **L7**.[13] We were however unable to obtain single crystals suitable for X-ray diffraction studies, and this is tentatively assigned to the existence of a mixture of facial and meridional isomers displaying similar shapes and physico-chemical properties. On the other hand, fragile solvated X-ray quality prisms were obtained for the 1 : 2 complexes $[Eu(\mathbf{L1})_2(CF_3SO_3)_2(H_2O)](CF_3SO_3)(C_3H_5N)_2(H_2O)$ (**6**) and $[Eu(\mathbf{L4})_2(CF_3SO_3)_2(H_2O)](CF_3SO_3)(THF)_{1.5}$ (**7**) upon reacting two equivalents of the corresponding ligands with $Eu(CF_3SO_3)_3\cdot4H_2O$ (1 eq) in propionitrile, respectively tetrahydrofuran, followed by ultra-slow diffusion of light petroleum ether.

Crystal and molecular structures of 6 and 7

In these compounds, Eu^{III} is co-ordinated by two tridentate ligands, two monodentate triflate anions and one water molecule to give the nine-co-ordinate cations $[Eu(\mathbf{L1})_2(CF_3SO_3)_2(H_2O)]^+$ and $[Eu(\mathbf{L4})_2(CF_3SO_3)_2(H_2O)]^+$. The un-complexed solvent molecules, the ionic triflates and some terminal methyl groups of the co-ordinated carboxamide units are disordered, but show no other feature of interest (see experimental section). In **7**, the co-ordinated water molecule acts as a donor (O1w) in a weak hydrogen bond with an accepting THF molecule (O1w ··· O1f = 2.691(9) Å, O1w–Hw ··· O1f = 141(4)°). Fig. 5 shows the numbering schemes for the two cations, and selected bond distances and angles are given in Table 2.

The molecular structures of the two cations are almost superimposable and possess a pseudo-twofold axis passing through Eu–O1w (Fig. 6). The Eu^{III} co-ordination geometry can be best described as a distorted pseudo-tricapped trigonal prism (TTP), analogous to those found in the triple-helical complexes $[Eu(\mathbf{L5})_3]^{3+}$,[9a] $[Eu(\mathbf{L6})_3]^{3+}$,[16] and $[Eu(\mathbf{L7})]^{3+}$,[13] but in which one wrapped ligand strand is replaced with three monodentate ligands (two triflate anions and one water molecule, Fig. 5). Consequently, N2a,O1b,O1d and O1a,N2b,O1c define the two trigonal faces of the prism, while N1a,N1b,O1w cap the three rectangular faces (Figs 5, 6). The classical geometrical analysis which measures the bending (ϕ), flattening (θ_i) and twist (ω_{ij}) of the tricapped trigonal prism [13,22] shows a slight bending along the pseudo-C_3 axis (ϕ = 170.7–170.9° for **6** and **7**, ϕ = 180° for an ideal TTP; Table S3, ESI †) which translates into a non-parallel arrangement of the two trigonal faces (12.0(2)° for **6** and 9.4(2)° for **7**). The flattening (θ_i) and twist (ω_{ij}) around the pseudo-C_3 axis are similar to those reported for $[Eu(\mathbf{L7})]^{3+}$ (Table S3, ESI),[13] and Eu^{III} lies in the intermediate plane defined by the capping atoms N1a,N1b,O1w (deviation 0.000(1)° for **6** and 0.014(1)° for **7**). Interestingly, the two tridentate ligands in $[Eu(\mathbf{Li})_2(CF_3SO_3)_2(H_2O)]^+$ adopt an antiparallel orientation reminiscent of the parent *mer*-$[Eu(\mathbf{Li})_3]^{3+}$ (*i.e.* the oxygen donor atom of each tridentate ligand belongs to one different trigonal face of the prisms, Fig. 6).

Both crystal structures show no evidence for contamination with the alternative isomer in which the two tridentate ligands

Table 2 Selected bond lengths [Å] and bond angles [°] in $[Eu(\mathbf{L1})_2(CF_3SO_3)_2(H_2O)](CF_3SO_3)(C_3H_5N)_2(H_2O)$ (**6**) and $[Eu(\mathbf{L4})_2(CF_3SO_3)_2(H_2O)](CF_3SO_3)(THF)_{1.5}$ (**7**)

	6			**7**	
	Ligand a	Ligand b		Ligand a	Ligand b
Eu–O1	2.386(3)	2.419(4)	Eu–O1	2.406(4)	2.405(4)
Eu–N1	2.610(4)	2.590(4)	Eu–N1	2.582(4)	2.592(5)
Eu–N2	2.557(4)	2.559(5)	Eu–N2	2.540(5)	2.551(5)
O1–Eu–N1	62.6(1)	63.4(1)	O1–Eu–N1	63.3(1)	63.4(1)
N1–Eu–N2	63.5(1)	62.3(1)	N1–Eu–N2	63.5(1)	62.1(2)
O1–Eu–N2	126.1(1)	125.6(1)	O1–Eu–N2	126.8(1)	125.2(2)
Eu–O1c	2.429(4)		Eu–O1c	2.420(5)	
Eu–O1d	2.496(3)		Eu–O1d	2.512(4)	
Eu–O1w	2.440(4)		Eu–O1w	2.433(4)	
O1c–Eu–O1w	72.2(1)		O1c–Eu–O1w	71.3(1)	
O1d–Eu–O1w	69.7(1)		O1d–Eu–O1w	68.4(1)	
O1c–Eu–O1d	140.8(1)		O1c–Eu–O1d	138.4(1)	

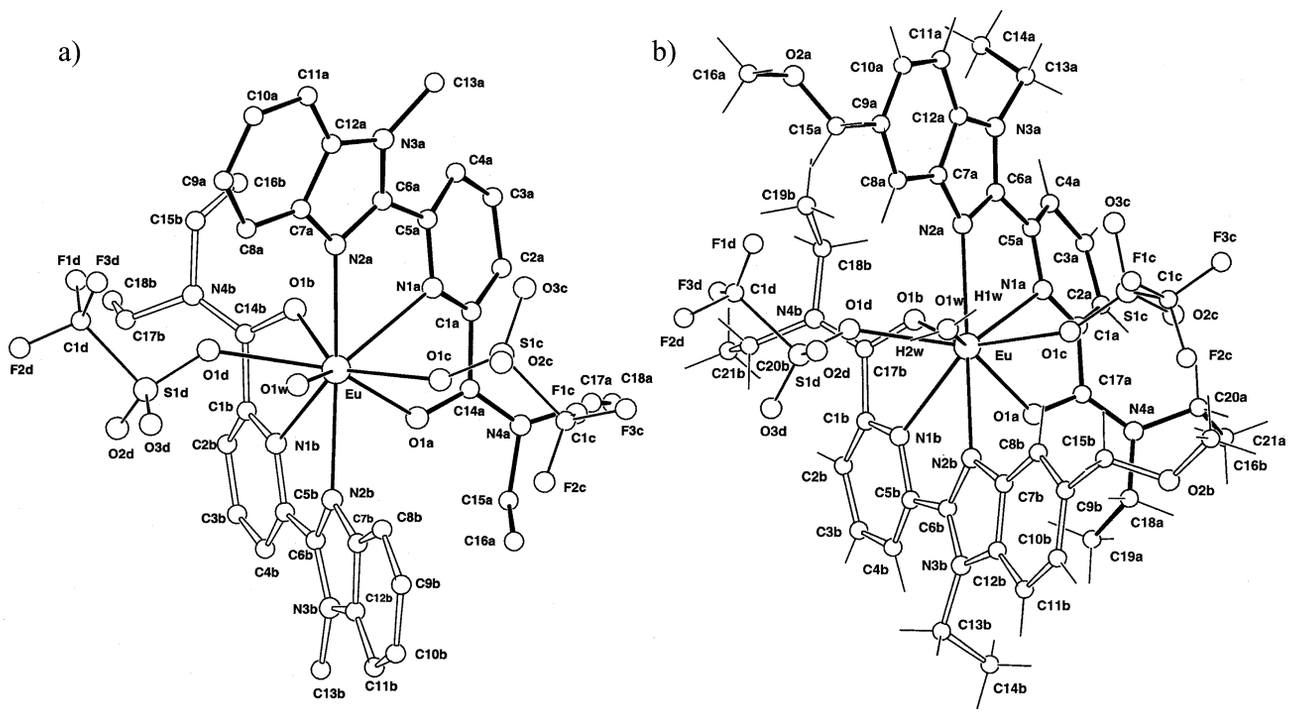

Fig. 5 ORTEP views of the molecular structures of the cations (a) $[Eu(\mathbf{L1})_2(CF_3SO_3)_2(H_2O)]^+$ (**6**) and (b) $[Eu(\mathbf{L4})_2(CF_3SO_3)_2(H_2O)]^+$ (**7**) along the Ln–O1w bond with atomic numbering scheme.

adopt a parallel orientation. The $Eu–O1_{amide}$ (2.386–2.419 Å, average: 2.40(1) Å) and the $Eu–N1_{py}$ (2.582–2.610 Å, average: 2.59(1) Å) in **6** and **7** are standard [16,23] and match those obtained for $[Eu(\mathbf{L7})]^{3+}$ ($Eu–O_{amide}$ 2.418(6) Å and $Eu–N_{py}$ = 2.602(7) Å).[13] This indicates that the covalent tripod in the latter complex induces negligible constraints on the binding of the terminal pyridine–carboxamide units. However, the $Eu–N2_{benzim}$ (2.540–2.559 Å, average: 2.551(8) Å) in $[Eu(\mathbf{Li})_2(CF_3SO_3)_2(H_2O)]^+$ are slightly shorter than 2.582(6) Å observed in $[Eu(\mathbf{L7})]^{3+}$ [13] and 2.58(1) Å reported in $[CrEu(\mathbf{L8})_3]^{6+}$ [23] which possess facial EuN_6O_3 metallic sites capped with a tripod. We conclude that the marginally shorter $Eu–N_{bzim}$ found in **6** and **7** reflects the standard bond length for tridentate *NNO* ligands such as **L1**–**L4** in absence of constraints imposed by the connection of the benzimidazole rings to a tripod. These values will be used for the parametrisation of the force field in molecular mechanic (*vide supra*). Finally, we note that the substitution at the 5-position of the benzimidazole ring in **L4** has negligible effect on bond lengths and geometries in the final 1:2 complexes.

Characterization of the *fac*-$[Ln(\mathbf{Li})_3]^{3+} \rightleftharpoons$ *mer*-$[Ln(\mathbf{Li})_3]^{3+}$ isomerisation in acetonitrile (Ln = La, Y, Lu; *i* = 1, 3, 4)

The lability of the helical $P \rightleftharpoons M$ interconversion process in $[Ln(\mathbf{L6})_3]^{3+}$ strongly decreases along the lanthanide series ($\Delta G^{\neq}_{La} << 55$ kJ mol^{-1}, $\Delta G^{\neq}_{Sm} = 55$ kJ mol^{-1}, $\Delta G^{\neq}_{Y} = 73$ kJ mol^{-1} and $\Delta G^{\neq}_{Lu} = 78$ kJ mol^{-1} at the coalescence temperatures, 263 (Sm), 318 (Y) and 333 K (Lu). The observation of D_3-symmetrical triple-helical complexes blocked on the ^{1}H-NMR time scale in the 233–333 K range is thus limited to small Ln^{III} in acetonitrile.[16] Although the facial/meridional isomerisation process involving unsymmetrical tridentate ligands in $[Ln(\mathbf{Li})_3]^{3+}$ (*i* = 1, 3, 4; eqn. 4) is more complicated than the simple helical interconversion described for the D_3-symmetrical triple-helical complexes $[Ln(\mathbf{L6})_3]^{3+}$, we similarly observe a fast interconversion on the NMR time scale in $[La(\mathbf{L4})_3]^{3+}$ leading to average C_{3v} or D_{3h}-symmetries characterized by fourteen ^{1}H NMR signals corresponding to a single ligand **L4** displaying enantiotopic methylene protons (10^{-2} mol dm^{-3}, CD_3CN, 233–333 K). This observation could result from the quantitative

Table 3 Distributions of *fac*-[Lu(**L*i***)$_3$]$^{3+}$ and *mer*-[Lu(**L*i***)$_3$]$^{3+}$ (*i*=1, 3, 4) and associated thermodynamic data according to eqn. 4 (total metal concentration: 10^{-2} M in CD_3CN)

T/K	*fac*-[Lu(**L1**)$_3$]$^{3+}$ (%)[a]	*mer*-[Lu(**L1**)$_3$]$^{3+}$ (%)[a]	K_4^{exp}	ΔG_4^{exp}/kJ mol^{-1}
233	5.9	94.1	15.9(8)	−5.4(1)
238	5.4	94.6	17.5(8)	−5.7(1)
243	5.9	94.1	15.9(8)	−5.6(1)
248	5.9	94.1	15.8(8)	−5.7(1)
253	6.0	94.0	15.7(8)	−5.8(1)
258	7.0	93.0	13.3(7)	−5.6(1)
263	6.9	93.1	13.4(7)	−5.7(1)
268	7.5	92.5	12.4(6)	−5.6(1)
273	7.4	92.6	12.5(6)	−5.7(1)
278	7.2	92.8	13.0(6)	−5.9(1)
288	8.5	91.5	10.8(5)	−5.7(1)
T/K	*fac*-[Lu(**L3**)$_3$]$^{3+}$ (%)[a]	*mer*-[Lu(**L3**)$_3$]$^{3+}$ (%)[a]	K_4^{exp}	ΔG_4^{exp}/kJ mol^{-1}
233	70.4	29.6	0.42(2)	1.67(8)
238	68.2	31.8	0.47(2)	1.51(8)
243	63.0	37.0	0.59(2)	1.07(8)
248	56.1	43.9	0.78(3)	0.51(8)
253	54.1	45.9	0.85(3)	0.34(8)
258	45.6	54.4	1.19(5)	−0.38(8)
T/K	*fac*-[Lu(**L4**)$_3$]$^{3+}$ (%)[a]	*mer*-[Lu(**L4**)$_3$]$^{3+}$ (%)[a]	K_4^{exp}	ΔG_4^{exp}/kJ mol^{-1}
238	9.0	91.0	10.2(5)	−4.6(1)
242	9.0	91.0	10.1(5)	−4.6(1)
253	13.0	87.0	6.7(3)	−4.0(1)
258	12.6	87.4	6.9(3)	−4.1(1)
263	12.1	87.9	7.3(4)	−4.3(1)
268	11.8	88.2	7.5(4)	−4.5(1)

[a] Obtained by integration of the ^{1}H NMR signals. The error is typically 0.5–1%.

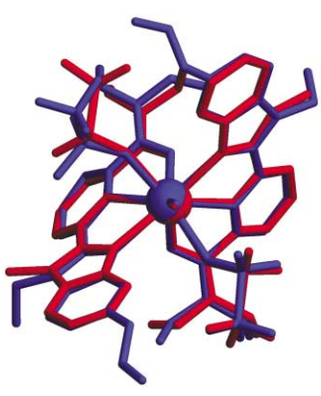

Fig. 6 Perspective view of the optimized superimposition of the two co-ordination spheres of [Eu(**L1**)$_2$(CF$_3$SO$_3$)$_2$(H$_2$O)]$^+$ (in red) and (b) [Eu(**L4**)$_2$(CF$_3$SO$_3$)$_2$(H$_2$O)]$^+$ (in blue) highlighting the pseudo-tricapped trigonal prismatic metallic sites.

formation of the facial C_3-symmetrical isomer *fac*-[La(**L4**)$_3$]$^{3+}$ exhibiting fast helical $P \rightleftharpoons M$ interconversion (average C_{3v}-symmetry), but the observation of a mixture of blocked *fac*-[Y(**L4**)$_3$]$^{3+}$ (14 signals) and *mer*-[Y(**L4**)$_3$]$^{3+}$ (42 signals) at 208 K (10^{-2} mol dm^{-3}, CD_3CN/CD_2Cl_2 1:1) strongly suggest that a similar mixture exists for Ln = La, and that a fast *fac* $\rightleftharpoons$ *mer* exchange process provides an average D_{3h}-symmetry on the NMR time scale.

$$fac\text{-}[Ln(\mathbf{Li})_3]^{3+} \rightleftharpoons mer\text{-}[Ln(\mathbf{Li})_3]^{3+}\ K_4^{exp} \qquad (4)$$

Despite the broadening of the signals observed in the low-temperature ^{1}H-NMR spectrum of *fac*-[Y(**L4**)$_3$]$^{3+}$ and *mer*-[Y(**L4**)$_3$]$^{3+}$ resulting from residual dynamic interconversion processes, a rough integration of the signals of the methyl protons gives 25% of *fac*-[Y(**L4**)$_3$]$^{3+}$ and 75% of *mer*-[Y(**L4**)$_3$]$^{3+}$ leading to K_4^{exp} = 3, in exact agreement with a simple statistical distribution exclusively controlled by the entropic contribution to eqn. 4: $\Delta S_4^{stat} = R \ln(3) = 19.1$ J mol^{-1} K^{-1}, $\Delta H_4^{stat} = 0$ kJ mol^{-1}, $\Delta G_4^{stat} = -T\Delta S_4^{stat} = -2.7$ kJ mol^{-1} at 298K and $K_4^{stat} = 3$.[5] For the smaller Lu^{III}, the facial/meridional interconversion process (eqn. 4) is slow enough to display blocked C_3-symmetrical *fac*-[Lu(**L4**)$_3$]$^{3+}$ and C_1-symmetrical *mer*-[Lu(**L4**)$_3$]$^{3+}$ on the NMR time scale in the range 233–273 K (Fig. 7). Interestingly, integrations at various temperature systematically show that the quantity of the meridional isomer (87–91%, $K_4^{exp} > 3$, Table 3) exceeds the statistical value (75%).

Application of the van't Hoff equation (eqn. 5) provides estimations for the enthalpic (ΔH_4^{exp}) and the entropic (ΔS_4^{exp}) contributions to ΔG_p^{exp} in [Lu(**L4**)$_3$]$^{3+}$ by plotting ln (K_4^{exp}) *versus* T^{-1} (Table 4, Fig. 8).

$$\ln\left(K_4^{exp}\right) = -\frac{\Delta H_4^{exp}}{R}\frac{1}{T} + \frac{\Delta S_4^{exp}}{R} \qquad (5)$$

The excess of *mer*-[Lu(**L4**)$_3$]$^{3+}$ corresponds to an extra free energy of stabilisation of $\Delta(\Delta G) = \Delta G_4^{exp} - \Delta G_4^{stat} \approx -2$ kJ mol^{-1} at 273 K (Table 3) which mainly results from a favorable enthalpic contribution $\Delta H_4^{exp} = -6.9(2.4)$ kJ mol^{-1} partially balanced by a negative entropy contribution (Table 4). Similar trend is observed for [Lu(**L1**)$_3$]$^{3+}$ in which the terminal methyl-eneoxymethyl group has been removed. The preference for the meridional isomer *mer*-[Lu(**L1**)$_3$]$^{3+}$ is marginally larger (91–94%) and leads to $\Delta(\Delta G) = \Delta G_4^{exp} - \Delta G_4^{stat} \approx -3.2$ kJ mol^{-1} at 273 K (Table 3) as a result of the favourable enthalpic term $\Delta H_4^{exp} = -4.3(5)$ kJ mol^{-1}. Since the accessible temperature range is very limited for applying eqn. 5, the entropic contribution cannot be safely interpreted, but the positive slopes observed for [Lu(**L4**)$_3$]$^{3+}$ and [Lu(**L1**)$_3$]$^{3+}$ (Fig. 8) unambiguously indicate that the meridional isomer is enthalpy stabilised (and/or the facial isomer destabilised) by some interstrand interactions which are neglected in the statistical approach ($\Delta H_4^{stat} = 0$ kJ mol^{-1}).

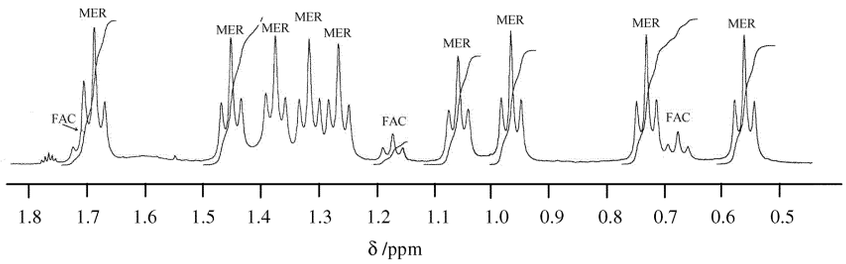

Fig. 7 Part of the 400 MHz ^{1}H NMR spectrum obtained for $[Lu(\mathbf{L4})_3]^{3+}$ showing the triplets of the terminal methyl groups of the three ethyl residues in *fac*-$[Lu(\mathbf{L4})_3]^{3+}$ (3 triplets) and *mer*-$[Lu(\mathbf{L4})_3]^{3+}$ (9 triplets; 10^{-2} mol dm^{-3}, CD_3CN, 238 K).

Table 4 Enthalpic and entropic contributions to *fac*-$[Lu(\mathbf{L}i)_3]^{3+} \rightleftharpoons$ *mer*-$[Lu(\mathbf{L}i)_3]^{3+}$ isomerisation (eqn. 4, i=1, 3, 4, CD_3CN) obtained by linear least-squares fits of eqn. 5

	$[Lu(\mathbf{L1})_3]^{3+}$	$[Lu(\mathbf{L3})_3]^{3+}$	$[Lu(\mathbf{L4})_3]^{3+}$
ΔH_4^{exp}/kJ mol^{-1}	−4.3(5)	21(2)	−6.9(2.4)
ΔS_4^{exp}/J mol^{-1} K^{-1}	5(5)	82(7)	−10(10)
$-T\Delta S_4^{exp}$/kJ mol^{-1}	−1.5(1.5)	−24(2)	3(3)

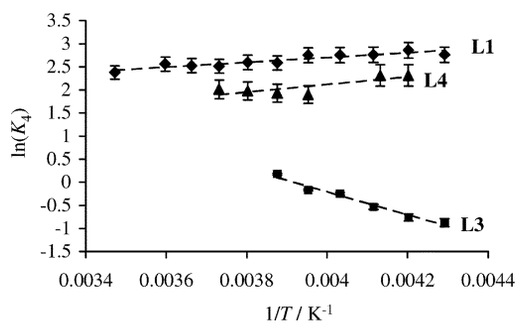

Fig. 8 Plots of ln (K_4^{exp}) *vs* T^{-1} for $[Lu(\mathbf{L}i)_3]^{3+}$ (i=1, 3, 4) according to eqn. 5.

According to Fig. 1, only the meridional isomer may lead to an intramolecular π-stacking interaction between the benzimidazole–pyridine units of two adjacent strands adopting an opposite orientation (Fig. 9*b*). This situation is well-known from the geometrical analysis of the related D_3-symmetrical complexes $[Lu(\mathbf{L5})_3]^{3+}$ which exhibit three such stacking interactions because each benzimidazole–pyridine unit of one ligand stacks with that of an adjacent strand.[9b,15] Such interaction is removed in the facial isomer (Fig. 1 and Fig. 9a) and it can be modulated in the meridional isomer with the introduction of bulky substituents bound to the benzimidazole rings.[9b,15] The 3,5-dimethoxybenzyl group in $[Lu(\mathbf{L3})_3]^{3+}$ has been introduced for this purpose and it indeed reverses the trend with a destabilisation of *mer*-$[Lu(\mathbf{L3})_3]^{3+}$ which forms 30–54% of the mixtures (K_4^{exp} < 3, Table 3). The dynamic of the facial/meridional process is faster with **L3** than with **L1** and **L4,** and blocked isomers on the NMR time scale are only observed in the 233–258 K range (Table 3). Unlike for $[Lu(\mathbf{L}i)_3]^{3+}$ (i = 1, 4), $\Delta(\Delta G) = \Delta G_4^{exp} - \Delta G_4^{stat}$ significantly varies with temperature for $[Lu(\mathbf{L3})_3]^{3+}$ (1.9 kJ mol^{-1} at 258 K ≤ $\Delta(\Delta G)$ = 3.8 kJ mol^{-1} at 233 K), which requires one to interpret both the large enthalpic contribution ΔH_4^{exp} = 21(2) kJ mol^{-1}, and the opposite entropic contribution ΔS_4^{exp} = 82(7) J mol^{-1} K^{-1} (Table 4, Fig. 8). The positive enthalpic contribution reflects the impossibility to pack two helical strands with opposite orientation in *mer*-$[Lu(\mathbf{L3})_3]^{3+}$ as a result of the steric congestion induced by the bulky 3,5-dimethoxybenzyl residues. Although large errors resulting from the minor accessible temperature range may affect the entropic contribution, its deviation from the statistical value $\Delta(\Delta S) = \Delta S_4^{exp} - \Delta S_4^{stat}$ = 82 − 9.1 ≈ 73 J mol^{-1} K^{-1} can be tentatively assigned to a more efficient solvation of *fac*-$[Lu(\mathbf{L3})_3]^{3+}$ resulting from the formation of an hydrophobic belt produced by the three bulky lipophilic substituents localised on the same side of the complex. This should allow an efficient solvation of the three polar carboxamide group by acetonitrile (a polar solvent), which is relaxed in *mer*-$[Lu(\mathbf{L3})_3]^{3+}$. This phenomenon is reminiscent of the unprecedented entropic stabilisation of 1 : 2 lanthanide capsules in which a peripheral hydrophobic belt prevent solvation by water molecules.[24]

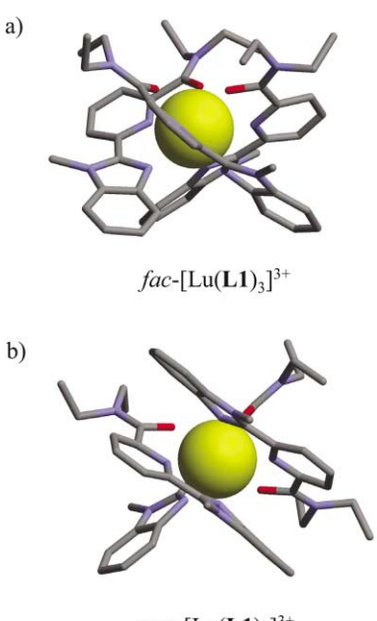

Fig. 9 Perspective views of the molecular structures of the two cations (a) *fac*-$[Lu(\mathbf{L1})_3]^{3+}$ and (b) *mer*-$[Lu(\mathbf{L1})_3]^{3+}$ obtained by molecular mechanics in the gas-phase.

Finally, we have performed a preliminary kinetic investigation of the dynamic facial/meridional process (eqn. 4) by using variable-temperature ^{1}H NMR. Coalescence of the four singlets corresponding to the isolated aromatic protons connected at the 4-position of the benzimidazole rings occurs at T_c = 323 K for $[Lu(\mathbf{L4})_3]^{3+}$ in CD_3CN, and we calculate with the *Eyring* model (eqns. 6–8)[25] that $\Delta G^{\neq}$ = 67(2) kJ mol^{-1} at 323 K (k is the rate constant at T_c, $\delta\nu$ = 46 Hz is the chemical shift difference in absence of exchange taken from the ^{1}H NMR data at 233 K, R, k_B and h are respectively the molar gas constant, the *Boltzmann* and *Planck* constants, Δp = 0.5 is the difference in population between the two exchangeable sites (approximately 25% *fac*-$[Lu(\mathbf{L4})_3]^{3+}$and 75% *mer*-$[Lu(\mathbf{L4})_3]^{3+}$ in the mixture), and X is the solution of the polynomial expression given in eqn. 8 (X = 2.30 for Δp = 0.5).[7,25]

$$\Delta G^{\neq} = RT \ln\left(\frac{k_B T}{kh}\right) \quad (6)$$

$$k = \frac{\pi\delta\nu}{X} \quad (7)$$

$$X^6 - 6X^4 + [12 - 27\,(\Delta p)^2]\,X^2 - 8 = 0 \quad (8)$$

Table 5 Average Ln–N and Ln–O bond distances determined by X-ray diffraction in $[Eu(\mathbf{L5})_3]^{3+}$, $[Eu(\mathbf{L6})_3]^{3+}$, $[Eu(\mathbf{L7})]^{3+}$, $[Eu(\mathbf{L1})_2(CF_3SO_3)_2(OH_2)]^{+}$ (**6**), $[Eu(\mathbf{L4})_2(CF_3SO_3)_2(OH_2)]^{+}$ (**7**) and $[EuCr(\mathbf{L8})_3]^{6+}$ and $[LuCr(\mathbf{L8})_3]^{6+}$, and those calculated by Molecular Mechanics (MM-Amber force field) for $[Eu(\mathbf{L5})_3]^{3+}$, $[Eu(\mathbf{L6})_3]^{3+}$, $[Lu(\mathbf{L1})_3]^{3+}$, $[Lu(\mathbf{L3})_3]^{3+}$ and $[Lu(\mathbf{L4})_3]^{3+}$

	Eu–O_{amide}/Å	Eu–$N_{pyridine}$/Å	Eu–N_{benzim}/Å	Ref.
$[Eu(\mathbf{L5})_3]^{3+}$	—	2.576	2.60	15
$[Eu(\mathbf{L6})_3]^{3+}$	2.41	2.56	—	16
$[Eu(\mathbf{L7})]^{3+}$	2.418	2.602	2.582	13
$[Eu(\mathbf{L1})_2(CF_3SO_3)_2(OH_2)]^{+}$	2.40	2.60	2.558	This work
$[Eu(\mathbf{L4})_2(CF_3SO_3)_2(OH_2)]^{+}$	2.406	2.59	2.55	This work
$[EuCr(\mathbf{L8})_3]^{6+}$	2.40	2.61	2.58	23*b*
$[LuCr(\mathbf{L8})_3]^{6+}$	2.32	2.53	2.51	23*b*
$[Eu(\mathbf{L5})_3]^{3+}$	—	2.54	2.51	MM[a]
$[Eu(\mathbf{L5})_3]^{3+}$	—	2.45	2.43	MM[b]
$[Eu(\mathbf{L6})_3]^{3+}$	2.38	2.72	—	MM[a]
$[Eu(\mathbf{L6})_3]^{3+}$	2.28	2.61	—	MM[b]
fac-$[Lu(\mathbf{L1})_3]^{3+}$	2.257	2.403	2.324	MM[a]
mer-$[Lu(\mathbf{L1})_3]^{3+}$	2.23	2.40	2.34	MM[a]
fac-$[Lu(\mathbf{L3})_3]^{3+}$	2.24	2.58	2.31	MM[a]
mer-$[Lu(\mathbf{L3})_3]^{3+}$	2.22	2.55	2.33	MM[a]
fac-$[Lu(\mathbf{L4})_3]^{3+}$	2.26	2.48	2.31	MM[a]
mer-$[Lu(\mathbf{L4})_3]^{3+}$	2.25	2.48	2.34	MM[a]

[a] Modelled with the Lennard-Jones parameters of Eu^{III} and Lu^{III} reported in ref. 31. [b] Modelled with the Lennard-Jones parameters of Eu^{III} reported in ref. 32.

This free energy barrier for the meridional/facial isomerisation (eqn. 4) is comparable with those reported for helical $P \rightleftharpoons M$ interconversion in $[Lu(\mathbf{L6})_3]^{3+}$ ($\Delta G^{\neq}$ = 78 kJ mol^{-1} in CD_3CN)[16] and $[Yb(2,6\text{-dipicolinate})_3]^{3-}$ ($\Delta G^{\neq}$ = 60(1) kJ mol^{-1} in D_2O),[7] which suggests closely related mechanisms involving significant bond extension and/or bond breaking.

Molecular mechanics modelling of the *fac*-$[Lu(\mathbf{Li})_3]^{3+} \rightleftharpoons$ *mer*-$[Lu(\mathbf{Li})_3]^{3+}$ isomerisation in the gas phase

In an attempt to rationalise the origin of the variable enthalpic contributions to eqn. 4, we have resorted to molecular mechanic simulations (MM) in the gas-phase by using the Amber force field, as implemented in HyperChem 5.1,[26] with standard parameters for all atoms except Lu^{III}. The atomic charges borne by the free ligands **L*i*** (i = 1, 3, 4, 5, 6) have been fitted to the electrostatic potentials according to the Merz–Singh–Kollman scheme.[27] These charges were calculated at the Hartree–Fock (HF) level on molecular structures optimized in their *cis–cis* conformations with the 6-31G* basis set.[28] Interestingly, the negative charge borne by the O donor atoms of the carboxamide groups do not strongly vary in the different ligands, but the charges borne by the heterocyclic N donor atoms are sensitive to the various substituents bound to the aromatic rings (Scheme 2).[29] A set of charge has been previously calculated for **L6** by using Amber atom types which provide similar values for the O donor atoms (−0.588), but a larger negative charge (−0.679) for the N atom.[30]

For the central lanthanide atoms, we have tested Lennard-Jones parameters of van Veggel and Reinhoudt[31] obtained by a Monte Carlo method, and those of Durand *et al.* derived from molecular dynamic calculations[32] in order to reproduce the molecular X-ray structures of $[Eu(\mathbf{L5})_3]^{3+}$ [15] and $[Eu(\mathbf{L6})_3]^{3+}$.[16] Comparison of the simulated gas-phase structures with the crystal structures show a better agreement with the parameters proposed by van Veggel and Reinhoudt (Fig. S1, ESI †).[31] The simulated Eu–N and Eu–O bond distances in $[Eu(\mathbf{L1})_2(CF_3SO_3)_2(H_2O)]^{+}$ (**6**) and $[Eu(\mathbf{L4})_2(CF_3SO_3)_2(H_2O)]^{+}$ (**7**) are also satisfyingly reproduced with these parameters which have been then used for optimizing *fac*-$[Lu(\mathbf{Li})_3]^{3+}$ and *mer*-$[Lu(\mathbf{Li})_3]^{3+}$ (i = 1, 3, 4; Table 5).

The starting structures of *fac*-$[Lu(\mathbf{Li})_3]^{3+}$and *mer*-$[Lu(\mathbf{Li})_3]^{3+}$ are identical except for the inversion of one tridentate binding unit. MM calculations converge to give the final optimised structures (Fig. 9, and Figs. S2 and S3, ESI), together with the associated total energies and their various contributions (Table 6). In all cases, the electrostatic contributions largely dominate the total energies and favour the facial isomer. However, the ultimate difference in energy between the two isomer favours *mer*-$[Lu(\mathbf{L1})_3]^{3+}$ ($\Delta E = E_{mer} - E_{fac}$ = −3.8 kJ mol^{-1}) and *mer*-$[Lu(\mathbf{L4})_3]^{3+}$ (ΔE = −2.5 kJ mol^{-1}), while *fac*-$[Lu(\mathbf{L3})_3]^{3+}$ is stabilised with ΔE = +17.6 kJ mol^{-1} (Table 6).

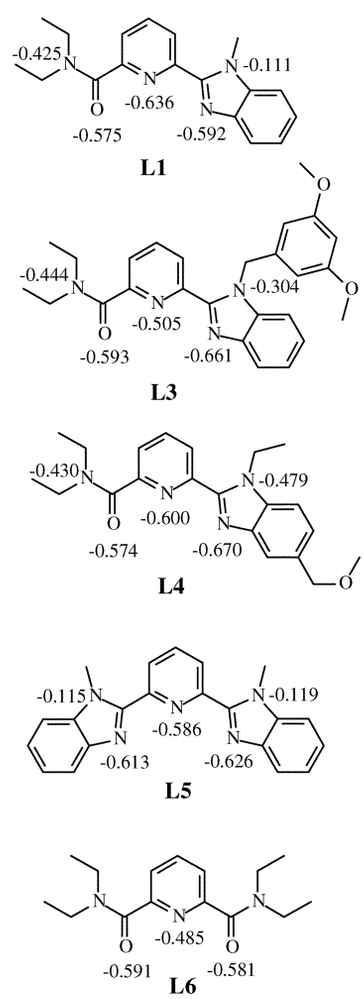

Scheme 2 Selected fitted partial charges[27] calculated at the HF level for the gas-phase optimized structures of **L1**, **L3**–**L6** in their *cis–cis* conformations with the 6-31G* basis set.

Table 6 Total simulated energy and its components obtained by molecular mechanics in the gas phase (MM-Amber force field) for *fac*-[Lu(**L*i***)$_3$]$^{3+}$ and *mer*-[Lu(**L*i***)$_3$]$^{3+}$ (*i* = 1, 3, 4)

	Total energy/ kJ mol^{-1}	Bond/ kJ mol^{-1}	Angle/ kJ mol^{-1}	Dihedral/ kJ mol^{-1}	VdWaals/ kJ mol^{-1}	Electrostatic/ kJ mol^{-1}
fac-[Lu(**L1**)$_3$]$^{3+}$	−2589.9	32.6	93.2	104.9	252.5	−3074.0
mer-[Lu(**L1**)$_3$]$^{3+}$	−2593.7	32.6	98.6	86.9	249.5	−3062.3
fac-[Lu(**L3**)$_3$]$^{3+}$	−3146.7	32.6	105.3	184.3	188.1	−3657.1
mer-[Lu(**L3**)$_3$]$^{3+}$	−3129.1	32.6	112.0	164.3	204.8	−3642.9
fac-[Lu(**L4**)$_3$]$^{3+}$	−2786.0	34.3	104.9	151.7	191.9	−3268.8
mer-[Lu(**L4**)$_3$]$^{3+}$	−2788.5	30.9	100.3	137.1	177.2	−3234.1

These predictions completely neglect entropic contributions, but they fairly match the trend observed for the experimental enthalpic contributions to eqn. 4 which amount to ΔH_4^{exp} = −4.3(5) kJ mol^{-1} ([Lu(**L1**)$_3$]$^{3+}$), ΔH_4^{exp} = −6.9(2.4) ([Lu(**L4**)$_3$]$^{3+}$) and ΔH_4^{exp} = 21(2) kJ mol^{-1} ([Lu(**L3**)$_3$]$^{3+}$, Table 4). Detailed geometrical analyses of the tricapped trigonal prismatic coordination spheres with the classical angles measuring bending (ϕ), flattening (θ_i) and twist (ω_{ij})[13,22] display only minor variations between the meridional and facial isomers of [Lu(**L*i***)$_3$]$^{3+}$ (*i* = 1, 4), and the trigonal distortions found in the simulated complexes (ω_{ij} = 10–15°) match those reported in [LuCr(**L8**)$_3$]$^{6+}$ (ω_{ij} = 9–10°).[23b] The main structural difference between *fac*-[Lu(**L*i***)$_3$]$^{3+}$and *mer*-[Lu(**L*i***)$_3$]$^{3+}$ (*i* = 1: Fig. 9, *i* = 4: Fig. S3, ESI) results from the roughly parallel arrangement of the pyridine–benzimidazole units of two adjacent strands displaying an opposite orientation in *mer*-[Lu(**L*i***)$_3$]$^{3+}$, which is not found in *fac*-[Lu(**L*i***)$_3$]$^{3+}$. We expect that this specific interaction in the meridional isomer provides a stabilising intramolecular π-stacking interaction reducing the overall van der Waals repulsion calculated for *mer*-[Lu(**L*i***)$_3$]$^{3+}$ (*i* = 1–4), which is smaller than that calculated for the analogous facial isomer (Table 6). The opposite situation is found with [Lu(**L3**)$_3$]$^{3+}$ in which the bulky 3,5-dimethoxybenzyl substituents perturb the regular wrapping of the strands (ω_{ij} = 15–21°) and prevent the parallel arrangement of benzimidazole–pyridine units in *mer*-[Lu(**L3**)$_3$]$^{3+}$ (Fig. S2, ESI). This produces a strong interstrand repulsion which increases the van der Waals destabilisation in *mer*-[Lu(**L3**)$_3$]$^{3+}$ (Table 6). In this context, we note that the pyridine rings are particularly tilted in the optimised structures of [Lu(**L3**)$_3$]$^{3+}$ (*i.e.* the lone pair of the nitrogen donor does not point toward Lu^{III}, Fig. S2, ESI), a phenomenon previously observed for [Ln(**L6**)$_3$]$^{3+}$ [16] and [Ln(2,6-dipicolinate)$_3$]$^{3-}$ (Ln = La–Eu)[7c] when the electrostatic Ln–N_{py} interaction is reduced by the less negative charge borne by the donor N-atom (Scheme 2). Although a more detailed analysis of steric constraints is out of the scope of our simple molecular mechanics modelling, we can conclude that electrostatic interactions favour the facial isomer, but a reduced steric congestion combined with the existence of an interstrand π-stacking interaction in the meridional isomer bearing small substituents may overcome this trend and leads to an enthalpic stabilisation of *mer*-[Lu(**L*i***)$_3$]$^{3+}$ (*i* = 1–4).

Conclusion

A current trend in metallosupramolecular chemistry is to limit the synthetic complexity of the receptors in order to obtain sophisticated self-assembled architectures with a minimum of efforts.[33] Our attempt to control the formation of facial/meridional isomers by using peripheral substitution addresses this point since any success in this field would avoid the design of helical tripod connected to three unsymmetrical tridentate binding units obtained by tedious multi-step strategies.[13,29] However, the removal of the capping tripod when going from [Ln(**L7**)]$^{3+}$ to [Ln(**L4**)$_3$]$^{3+}$ has dramatic structural, kinetic and thermodynamic consequences. Firstly, while the helical interconversion *P*-[Ln(**L7**)]$^{3+}$ ⇌ *M*-[Ln(**L7**)]$^{3+}$ is blocked on the NMR time scale in acetonitrile along the complete lanthanide series and in the 233–333 K range,[13] the *fac*-[Ln(**L4**)$_3$]$^{3+}$ ⇌ *mer*-[Ln(**L4**)$_3$]$^{3+}$ interconversion is fast on the NMR time scale except for Ln = Lu below room temperature ($\Delta G^{\neq}$ = 67 ± 2 kJ mol^{-1}), which prevents kinetics separation of these isomers on the laboratory scale. Secondly, our thermodynamic data suggest that the formation constants of [Ln(**L*i***)$_3$]$^{3+}$ (*i* = 1–4) possessing unsymmetrical *NNO* binding units are significantly less stable than the analogous D_3-symmetrical complexes [Ln(**L*i***)$_3$]$^{3+}$ (*i* = 5, 6) with symmetrical *NNN* or *ONO* donor sets respectively. In the absence of specific entropic and enthalpic contributions to the free energies of formation, the origin of this effect remains elusive, but it contributes to favour the use of a tripod for maximizing the pre-organisation of poorly co-ordinating unsymmetrical binding units. Finally the distribution of *fac*-[Lu(**L*i***)$_3$]$^{3+}$and *mer*-[Lu(**L*i***)$_3$]$^{3+}$ (*i* = 1, 3, 4) investigated on the millisecond time scale by ^{1}H NMR in solution surprisingly shows that the statistical model based on (i) a pure entropic stabilisation of the meridional isomer and (ii) similar enthalpic contents for the two isomers is not followed. For [Lu(**L*i***)$_3$]$^{3+}$ (*i* = 1, 4), the absence of bulky substituents on the benzimidazole rings allows an interstrand π-stacking interaction in *mer*-[Lu(**L*i***)$_3$]$^{3+}$ which contributes to its enthalpic stabilisation, an observation supported by our simple MM calculations, and by the 5 kJ mol^{-1} stabilising energy estimated for the offset π-stacking of two porphyrin rings.[34] For [Lu(**L3**)$_3$]$^{3+}$, the introduction of the bulky 3,5-dimethoxybenzyl group indeed induces the predicted enthalpic destabilisation of the meridional isomer resulting from the steric congestion between the parallel aromatic pyridine–benzimidazole units. However, the concomitant (and opposite) large entropic stabilisation of the same meridional isomer exemplifies the subtle effects which must be first rationalised for providing satisfying structural programming. Nevertheless, we demonstrate quantitatively in this contribution that intramolecular interstrand interactions are of crucial importance for controlling (i) the geometry and (ii) the stability of triple-helical lanthanide complexes although the metallic centres display no stereochemical preference. This opens interesting perspectives for the preparation of single isomers as building blocks for luminescent lanthanide-containing liquid crystals,[35] and for the control of *HHH*/*HHT* isomerisation in bimetallic helicates.[10]

Experimental

Solvents and starting materials

These were purchased from Fluka AG (Buchs, Switzerland) and used without further purification unless otherwise stated. The tridentate ligands **L1**,[11] **L2**,[12] **L3** [11] and **L4** [13] were obtained according to literature procedures. The triflate salts Ln(CF_3SO_3)$_3$·*x*H_2O and perchlorate salts Ln(ClO_4)$_3$·*x*H_2O (Ln = La–Lu) were prepared from the corresponding oxides (Rhodia, 99.99%) and dried according to published procedures.[36] The Ln content of solid salts was determined by complexometric titrations with Titriplex III (Merck) in the presence of urotropine and xylene orange.[37]

Caution. Dry perchlorates may explode and should be handled in small quantities and with the necessary precautions.[38]

Table 7 Summary of crystal data for $[Eu(\mathbf{L1})_2(CF_3SO_3)_2(H_2O)](CF_3SO_3)(C_3H_5N)_2(H_2O)$ (**6**) and $[Eu(\mathbf{L4})_2(CF_3SO_3)_2(H_2O)](CF_3SO_3)(THF)_{1.5}$ (**7**)

	6	**7**
Formula	$C_{45}H_{54}EuF_9N_{10}O_{13}S_3$	$C_{51}H_{66}EuF_9N_8O_{15.5}S_3$
Mol. wt.	1362.2	1458.4
Crystal system	Monoclinic	Triclinic
Space group	$P2_1/c$	$P\bar{1}$
a/Å	12.9334(12)	11.6156(6)
b/Å	34.961(3)	13.2032(9)
c/Å	14.0207(13)	22.0941(13)
α/°	90	99.425(7)
β/°	113.229(10)	103.063(7)
γ/°	90	99.410(7)
U/Å^3	5826(1)	3184.5(4)
Z	4	2
μ(Mo Kα)/mm^{-1}	1.279	1.177
No. measured reflc.	42143	29939
No. unique reflc.	11119	11619
No. observed reflc.	7241	6920
R, ωR	0.045, 0.041	0.041, 0.040

Preparation of the complexes with L2 and L4

A solution of $Ln(ClO_4)_3 \cdot xH_2O$ or $Ln(CF_3SO_3)_3 \cdot xH_2O$ (Ln = Eu, Tb, Lu; 0.062 mmol) in acetonitrile (1 cm^3) was added to a solution of **L*i*** (0.186 mmol) in acetonitrile (1 cm^3). After stirring for 2 h at RT, amorphous powders of $[Ln(\mathbf{L2})_3](ClO_4)_3 \cdot xH_2O$ (Ln = Eu, x = 4: **1**; Ln = Tb, x = 5.5: **2**; Ln = Lu, x = 4: **3**) and $[Ln(\mathbf{L4})_3](CF_3SO_3)_3 \cdot xC_7H_{15}$ (Ln = Eu, x = 0: **4**; Ln = Lu, x = 0.4: **5**) were obtained by precipitation with diethyl ether (**1**–**3**) or heptane (**4**–**5**) in 45–70% yield. All the complexes were characterized by their IR spectra and gave satisfying analyses (Table S2, ESI†). Fragile solvated monocrystals of the 1 : 2 complexes $[Eu(\mathbf{L1})_2(CF_3SO_3)_2(H_2O)](CF_3SO_3)(C_3H_5N)_2(H_2O)$ (**6**) and $[Eu(\mathbf{L4})_2(CF_3SO_3)_2(H_2O)](CF_3SO_3)(THF)_{1.5}$ (**7**), suitable for X-ray diffraction studies, were obtained upon reacting two equivalents of the corresponding ligands **L1** or **L4** with $Eu(CF_3SO_3)_3 \cdot 4H_2O$ (1 eq) in propionitrile or tetrahydrofuran, respectively, followed by ultra-slow diffusion of light petroleum ether.

Crystal-structure determinations of $[Eu(\mathbf{L1})_2(CF_3SO_3)_2(H_2O)](CF_3SO_3)(C_3H_5N)_2(H_2O)$ (6) and $[Eu(\mathbf{L4})_2(CF_3SO_3)_2(H_2O)](CF_3SO_3)(THF)_{1.5}$ (7)

Summary of crystal data, intensity measurements and structure refinement are collected in Table 7. The crystals were mounted on quartz fibres with protection oil. Cell dimensions and intensities were measured at 200 K on a Stoe IPDS diffractometer with graphite-monochromated Mo Kα radiation (λ = 0.71073 Å). Data were corrected for Lorentz and polarization effects and for absorption. The structure were solved by direct methods (SIR97),[39] all other calculations were performed with XTAL[40] system and ORTEP[41] programs.

$[Eu(\mathbf{L1})_2(CF_3SO_3)_2(H_2O)](CF_3SO_3)(C_3H_5N)_2(H_2O)$ (6). The hydrogen atoms of the methyl groups, of the propionitrile molecules and of the co-ordinated water molecule were refined with restraints on bond distances and bond angles. The other hydrogen atoms were placed in calculated positions and contributed to *Fc* calculations. Each methyl group C16a and C16b was disordered and refined on two different positions with population parameters of 0.70/0.30.

$[Eu(\mathbf{L4})_2(CF_3SO_3)_2(H_2O)](CF_3SO_3)(THF)_{1.5}$ (7). The hydrogen atoms of the co-ordinated water molecule were refined with restraints on bond distances and bond angles. The other hydrogen atoms were placed in calculated positions and contributed to *Fc* calculations. The methyl group C19*b* is disordered and was refined on two different positions with population parameters of 0.70/0.30. The two THF molecules **f** and **g** are also disordered. The oxygen atom of molecule **f** (PP = 1) was involved as an acceptor in a hydrogen bond. The carbon atoms are disordered and refined on eight sites with PP = 0.5. The molecule **g** is disordered around a centre of inversion (PP = 0.5).

CCDC reference numbers 225108 (**6**), 225109 (**7**).

See http://www.rsc.org/suppdata/dt/b3/b316035a/ for crystallographic data in CIF or other electronic format.

Spectroscopic and analytical measurements

Electronic spectra in the UV-Vis were recorded at 293 K from solutions in MeCN with a Perkin-Elmer Lambda 900 spectrometer using quartz cells of 0.1 and 1 mm path length. Spectrophotometric titrations were performed with a J&M diode array spectrometer (Tidas series) connected to an external computer. In a typical experiment, 50 cm^3 of **L1** in acetonitrile (2 10^{-4} mol dm^{-3}) were titrated at 20 °C with an equimolar solution of $Ln(ClO_4)_3 \cdot xH_2O$ (10^{-3} mol dm^{-3}) in acetonitrile under an inert atmosphere. After each addition of 0.20 ml, the absorbance was recorded using Hellma optrodes (optical path length 0.1 cm) immersed in the thermostated titration vessel and connected to the spectrometer. Mathematical treatment of the spectrophotometric titrations was performed with factor analysis[14] and with the SPECFIT program.[17] IR spectra were obtained from KBr pellets with a Perkin Elmer 883 spectrometer or with a Mattson α-Centauri FT-IR spectrometer. ^{1}H and ^{13}C NMR spectra were recorded at 25 °C on a Broadband Varian Gemini 300 spectrometer or on a Bruker AMX 400. Chemical shifts are given in ppm with respect to TMS. Excitation and emission spectra as well as lifetime measurements were recorded on a Perkin-Elmer LS-50B spectrometer equipped for low-temperature measurements. The quantum yields Φ have been calculated using the equation

$$\frac{\Phi_x}{\Phi_r} = \frac{A_r(\tilde{\nu})I_r(\tilde{\nu})n_x^2 D_x}{A_x(\tilde{\nu})I_x(\tilde{\nu})n_r^2 D_r}$$

where x refers to the sample and r to the reference; A is the absorbance, $\tilde{\nu}$ the excitation wavenumber used, I the intensity of the excitation light at this energy, n the refractive index and D the integrated emitted intensity.[42] $[Eu(terpy)_3](ClO_4)_3$ (Φ_{tot}^{Eu} = 1.3%, acetonitrile, 10^{-3} mol dm^{-3}) and $[Tb(terpy)_3](ClO_4)_3$ (Φ_{tot}^{Tb} = 4.7%, acetonitrile, 10^{-3} mol dm^{-3}) were used as references for the determination of quantum yields of respectively Eu- and Tb-containing samples.[19,43] Quantum yields of the ligand-centred emission were measured relative to quinine sulfate in 0.05 M H_2SO_4 (A_{347} = 0.05, absolute quantum yield: 0.546).[44] Elemental analyses were performed by Dr. H. Eder from the Microchemical Laboratory of the University of Geneva.

Computational details

All the MM geometry optimizations have been perfomed using the HyperChem 5.1[26] program with standard Amber force field parameters for all atoms except for Eu^{III} and Lu^{III} taken from ref. 31. The atomic fitted charges borne by the free ligands L*i* (i = 1, 3–6) as well as the Hartree–Fock optimized molecular structures have been calculated with the 6-31G* basis set using the Gaussian 98 package.[28] Silicon graphics O2 and Origin 200 workstations have been used to do all the computations.

Acknowledgements

Financial support from the Swiss National Science Foundation, National Research Programme 47 'Supramolecular Functional Materials' is gratefully acknowledged. We thank Hélène Lartigue and Bernard Bocquet for technical support.

References

1 A. Werner, *Chem. Ber.*, 1911, **44**, 1887.
2 For recent reviews, see (*a*) F. R. Keene, *Coord. Chem. Rev.*, 1997, **166**, 121; (*b*) U. Knopf and A. von Zelewsky, *Angew. Chem., Int. Ed.*, 1999, **38**, 302; (*c*) A. von Zelewsky and O. Mamula, *J. Chem. Soc., Dalton Trans.*, 2000, 219.
3 (*a*) L. J. Charbonnière, A. F. Williams, U. Frey, A. E. Merbach, P. Kamalaprija and O. Schaad, *J. Am. Chem. Soc.*, 1997, **119**, 2488; (*b*) M. Gromova, O. Jarjayes, S. Hamman, R. Nardin, C. Béguin and R. Willem, *Eur. J. Inorg. Chem.*, 2000, 545; (*c*) M. Utz, C.-L. Chen, M. Morton and F. Papadimitrakopoulos, *J. Am. Chem. Soc.*, 2003, **125**, 1371.
4 (*a*) Y. Yoshikawa and K. Yamasaki, *Coord. Chem. Rev.*, 1979, **28**, 205; (*b*) N. C. Fletcher and F. R. Keene, *J. Chem. Soc., Dalton Trans.*, 1999, 683; (*c*) J. Lacour and V. Hebbe-Viton, *Chem. Soc. Rev.*, 2003, **32**, 373 and references therein.
5 (*a*) N. C. Fletcher, M. Nieuwenhuyzen and S. Rainey, *J. Chem. Soc., Dalton Trans.*, 2001, 2641; (*b*) A. B. Tamayo, B. D. Alleyne, P. I. Djurovich, S. Lamansky, I. Tsyba, N. H. Ho, R. Bau and M. E. Thompson, *J. Am. Chem. Soc.*, 2003, **125**, 7377.
6 (*a*) A. Juris, S. Barigelletti, S. Campagna, V. Balzani, P. Belser and A. von Zelewsky, *Coord. Chem. Rev.*, 1988, **84**, 85; (*b*) M. Meyer, B. Kersting, R. E. Powers and K. N. Raymond, *Inorg. Chem.*, 1997, **36**, 5179; (*c*) M. Albrecht and M. Schneider, *Chem. Commun.*, 1997, 137; (*d*) T. Konno, Y. Chikamoto, K.-I. Okamoto, T. Yamaguchi, T. Ito and M. Hitotsu, *Angew. Chem., Int. Ed.*, 2000, **39**, 4098; (*e*) X. Sun, D. W. Johnson, D. L. Caulder, K. N. Raymond and E. H. Wong, *J. Am. Chem. Soc.*, 2001, **123**, 2752.
7 (*a*) E. Huskowska and J. P. Riehl, *Inorg. Chem.*, 1995, **34**, 5615; (*b*) S. C. J. Meskers and H. P. J. M. Dekkers, *J. Phys. Chem. A*, 2001, **105**, 4589; (*c*) N. Ouali, B. Bocquet, S. Rigault, P.-Y. Morgantini, J. Weber and C. Piguet, *Inorg. Chem.*, 2002, **41**, 1436.
8 (*a*) C. Görller-Walrand and K. Binnemans, in *Handbook on the Physics and Chemistry of Rare Earths*, ed. K. A. Gschneidner, Jr. and L. Eyring, North-Holland Publishing Company, Amsterdam, 1996, vol. 23, pp. 121–283; (*b*) C. Görller-Walrand and K. Binnemans, in *Handbook on the Physics and Chemistry of Rare Earths*, ed. K. A. Gschneidner, Jr. and L. Eyring, North-Holland Publishing Company, Amsterdam, 1998, vol. 25, pp. 101–264; (*c*) J.-C. G. Bünzli and C. Piguet, *Chem. Rev.*, 2002, **102**, 1897.
9 (*a*) S. Petoud, J.-C. G. Bünzli, F. Renaud, C. Piguet, K. J. Schenk and G. Hopfgartner, *Inorg. Chem.*, 1997, **36**, 5750; (*b*) T. LeBorgne, J.-M. Bénech, S. Floquet, G. Bernardinelli, C. Aliprandini, P. Bettens and C. Piguet, *Dalton Trans.*, 2003, 3856.
10 (*a*) C. Piguet, G. Bernardinelli and G. Hopfgartner, *Chem. Rev.*, 1997, **97**, 2005; (*b*) M. Albrecht, *Chem. Rev.*, 2001, **101**, 3457; (*c*) N. André, R. Scopelliti, G. Hopfgartner, C. Piguet and J.-C. G. Bünzli, *Chem. Commun.*, 2002, 214; (*d*) N. André, R. Scopelliti, D. Imbert, M. Elhabiri, G. Hopfgartner, C. Piguet and J.-C. G. Bünzli, *Inorg. Chem.*, 2004, **43**, 515.
11 C. Piguet, B. Bocquet and G. Hopfgartner, *Helv. Chim. Acta*, 1994, **77**, 931.
12 N. Martin, J.-C. G. Bünzli, V. McKee, C. Piguet and G. Hopfgartner, *Inorg. Chem.*, 1998, **37**, 577.
13 S. Koeller, G. Bernardinelli and C. Piguet, *Dalton Trans.*, 2003, 2395.
14 E. R. Malinowski and D. G. Howery, *Factor Analysis in Chemistry*, Wiley, New York–Chichester, 1980.
15 C. Piguet, J.-C. G. Bünzli, G. Bernardinelli and A. F. Williams, *Inorg. Chem.*, 1993, **32**, 4139.
16 F. Renaud, C. Piguet, G. Bernardinelli, J.-C. G. Bünzli and G. Hopfgartner, *Chem. Eur. J.*, 1997, **3**, 1646.
17 (*a*) H. Gampp, M. Maeder, C. J. Meyer and A. D. Zuberbühler, *Talanta*, 1986, **33**, 943; (*b*) H. Gampp, M. Maeder, C. J. Meyer and A. D. Zuberbühler, *Talanta*, 1985, **23**, 1133.
18 G. R. Choppin, in *Lanthanide Probes in Life, Chemical and Earth Sciences*, ed. J.-C. G. Bünzli and G. R. Choppin, Elsevier, Amsterdam, ch. 1, 1989.
19 S. Petoud, J.-C. G. Bünzli, C. Piguet, Q. Xiang and R. Thummel, *J. Lumin.*, 1999, **82**, 69.
20 (*a*) S. Tobita, M. Arakawa and I. Tanaka, *J. Phys. Chem.*, 1984, **88**, 2697; (*b*) S. Tobita, M. Arakawa and I. Tanaka, *J. Phys. Chem.*, 1985, **89**, 5649.
21 J.-C. G. Bünzli, in *Lanthanide Probes in Life, Chemical and Earth Sciences*, ed. J.-C. G. Bünzli and G. R. Choppin, Elsevier, Amsterdam, ch. 7, 1989.
22 C. Piguet, J.-C. G. Bünzli, G. Bernardinelli, C. G. Bochet and P. Froidevaux, *J. Chem. Soc., Dalton Trans.*, 1995, 83.
23 (*a*) S. Rigault, C. Piguet, G. Bernardinelli and G. Hopfgartner, *J. Chem. Soc., Dalton Trans.*, 2000, 4587; (*b*) M. Cantuel, G. Bernardinelli, D. Imbert, J.-C. G. Bünzli, G. Hopfgartner and C. Piguet, *J. Chem. Soc., Dalton Trans.*, 2002, 1929.
24 M. P. Lowe, P. Caravan, S. J. Rettig and C. Orvig, *Inorg. Chem.*, 1998, **37**, 1637.
25 M. Pons and O. Millet, *Prog. Nucl. Magn. Reson. Spec.*, 2001, **38**, 267.
26 *HyperChem™ 5.11*, Hypercube, Inc., Gainesville, FL, 1998.
27 (*a*) B. H. Besler, K. M. Merz, Jr. and P. A. Kollman, *J. Comput. Chem.*, 1990, **11**, 431; (*b*) U. C. Singh and P. A. Kollman, *J. Comput. Chem.*, 1984, **5**, 129.
28 M. J. Frisch, G. W. Trucks, H. B. Schlegel, G. E. Scuseria, M. A. Robb, J. R. Cheeseman, V. G. Zakrzewski, J. A. Montgomery, Jr., R. E. Stratmann, J. C. Burant, S. Dapprich, J. M. Millam, A. D. Daniels, K. N. Kudin, M. C. Strain, O. Farkas, J. Tomasi, V. Barone, M. Cossi, R. Cammi, B. Mennucci, C. Pomelli, C. Adamo, S. Clifford, J. Ochterski, G. A. Petersson, P. Y. Ayala, Q. Cui, K. Morokuma, D. K. Malick, A. D. Rabuck, K. Raghavachari, J. B. Foresman, J. Cioslowski, J. V. Ortiz, B. B. Stefanov, G. Liu, A. Liashenko, P. Piskorz, I. Komaromi, R. Gomperts, R. L. Martin, D. J. Fox, T. Keith, M. A. Al-Laham, C. Y. Peng, A. Nanayakkara, C. Gonzalez, M. Challacombe, P. M. W. Gill, B. G. Johnson, W. Chen, M. W. Wong, J. L. Andres, M. Head-Gordon, E. S. Replogle and J. A. Pople, GAUSSIAN 98 (Revision A.7), Gaussian, Inc., Pittsburgh, PA, 1998.
29 J.-M. Senegas, G. Bernardinelli, D. Imbert, J.-C. G. Bünzli, P.-Y. Morgantini, J. Weber and C. Piguet, *Inorg. Chem.*, 2003, **42**, 4680.
30 M. Baaden, F. Berny, C. Madic and G. Wipff, *J. Phys. Chem. A*, 2000, **104**, 7659.
31 F. C. J. M. Van Veggel and D. N. Reinhoudt, *Chem. Eur. J.*, 1999, **5**, 90.
32 S. Durand, J.-P. Dognon, P. Guilbaud, C. Rabbe and G. Wipff, *J. Chem. Soc., Perkin 2*, 2000, 705.
33 M. J. Hannon, C. L. Painting, A. Jackson, J. Hamblin and W. Errington, *Chem. Commun.*, 1997, 1807; (*a*) L. J. Childs, N. W. Alcock and M. J. Hannon, *Angew. Chem., Int. Ed.*, 2002, **41**, 4244.
34 (*a*) C. A. Hunter, *Chem. Soc. Rev.*, 1994, 101 and references therein; (*b*) C. A. Hunter, K. R. Lawson, J. Perkins and C. J. Urch, *J. Chem. Soc., Perkin 2*, 2001, 651.
35 (*a*) K. Binnemans and C. Görller-Walrand, *Chem. Rev.*, 2002, **102**, 2303; (*b*) E. Terazzi, J.-M. Bénech, J.-P. Rivera, G. Bernardinelli, B. Donnio, D. Guillon and C. Piguet, *Dalton Trans.*, 2003, 769; (*c*) S. Suarez, O. Mamula, D. Imbert, C. Piguet and J.-C. G. Bünzli, *Chem. Commun.*, 2003, 1226.
36 J. F. Desreux, in *Lanthanide Probes in Life, Chemical and Earth Sciences*, ed. J.-C. G. Bünzli and G. R. Choppin, Elsevier, Amsterdam, 1989, ch. 2, p. 43.
37 G. Schwarzenbach, *Complexometric Titrations*, Chapman & Hall: London, 1957, p. 8.
38 (*a*) W. C. Wolsey, *J. Chem. Educ.*, 1978, **50**, A335; (*b*) W. R. Robinson, *J. Chem. Educ.*, 1985, **62**, 1001; (*c*) P. Patanaik, *Hazardous properties of chemical substances*, 2nd edn., John Wiley & Sons, New York, 1999.
39 A. Altomare, M. C. Burla, M. Camalli, G. Cascarano, C. Giacovazzo, A. Guagliardi, A. G. G. Moliterni, G. Polidori and R. Spagna, *J. Appl. Crystallogr.*, 1999, **32**, 115.
40 *XTAL 3.2 User's Manual*, ed. S. R. Hall, H. D. Flack and J. M. Stewart, Universities of Western Australia, Geneva and Maryland, 1992.
41 C. K. Johnson, *ORTEP II; Report ORNL-5138*, Oak Ridge National Laboratory, Oak Ridge, TN, 1976.
42 M. H. V. Werts, R. T. F. Jukes and J. W. Verhoeven, *Phys. Chem. Chem. Phys.*, 2002, **4**, 1542.
43 F. Renaud, C. Piguet, G. Bernardinelli, J.-C. G. Bünzli and G. Hopfgartner, *J. Am. Chem. Soc.*, 1999, **121**, 9326.
44 S. R. Meech and D. C. Phillips, *J. Photochem.*, 1983, **23**, 193–217.
45 R. D. Shannon, *Acta Crystallogr., Sect. A*, 1976, **32**, 751.